Magnetic exchange interactions of rare-earth-substituted DyCrO_{3} bulk powders

A. McDannald, L. Kuna, M. S. Seehra, and M. Jain

Phys. Rev. B **91**, 224415 — Published 11 June 2015

DOI: 10.1103/PhysRevB.91.224415

Study of Magnetic Exchange Interactions of Rare-Earth Substituted $DyCrO_3$ Bulk Powders

A. McDannald[1], L. Kuna[2], M. S. Seehra[3], and M. Jain[2,4,*]

[1]Materials Science and Engineering Department, University of Connecticut, Storrs, CT 06269
[2]Department of Physics, University of Connecticut, Storrs, CT 06269
[3] Department of Physics and Astronomy, West Virginia University, Morgantown, WV 26506
[4]Institute of Material Science, University of Connecticut, Storrs, CT 06269

Abstract:

Effects of the substitution of rare-earths R = Y, Er, and Ho on the magnetic properties of $Dy_{0.7}R_{0.3}CrO_3$ are reported here in order to probe the nature of magnetism and related exchange interactions in these materials. By fitting the temperature dependence of the magnetic susceptibility to a modified Curie-Weiss law, which includes a correction for the Dzyaloshinskii-Moriya (DM) interaction, the strengths of the symmetric and antisymmetric Cr^{3+}-Cr^{3+} exchange interactions were determined. It was found that the rare-earth substitutions had a slight effect on the strength of the symmetric Cr^{3+}-Cr^{3+} interaction (reflected in the slight changes in the Néel temperatures) while the antisymmetric Cr^{3+}-Cr^{3+} interaction remained unchanged. Isothermal magnetic measurements of the samples at successive temperatures revealed a plateau in the temperature dependent magnetic coercivity data, which was explained by the magnetic properties of the substituted ions. It was found that the Y substitution lead to the reduction of the strength of the magnetization and a larger peak value of magnetic coercivity as compared to that in pure $DyCrO_3$. The observed increase in coercivity with Er and Ho substitution can be attributed to an increased R^{3+}-Cr^{3+} interaction strength dominated by the DM mechanism.

*Author to whom correspondence should be addressed

I. Introduction:

Single phase magnetoelectric muliferroics (ME MFs) simultaneously exhibit both magnetic and ferroelectric orders. Such single phase ME MFs have been classified by D. Khomskii, among others, into two categories. [1–3] Type I ME MFs, such as $BiFeO_3$, are those in which magnetic and ferroelectric ordering temperatures occur at different temperatures and those can be above room temperature (hence it can show ferroelectric and magnetic properties at room temperature). [2] The main disadvantage with this class of ME MFs is that their ME coupling is usually weak due to different ordering mechanisms. Type II ME MFs (such as $TbMnO_3$), on the other hand have intrinsically high ME coupling as the ferroelectricity is believed to be induced by some magnetic order in the material. [4,5] However, this magnetically driven ferroelectricity typically commences at cryogenic temperatures (for example ~ 27 K for $TbMnO_3$). [4,5] ME MFs with strong ME coupling at ambient temperature have great potential for their applications in novel low-power RAM architectures, new programmable, low-power logic gate designs, etc. [6,7] Thus in order to design such ME MFs suitable for these applications, either the ordering temperatures of Type II ME MFs needs to be increased or the ME coupling in Type I ME MFs need to be enhanced.

Rare-earth chromites ($RCrO_3$) are an emerging class of ME MF materials in which the reported onset temperatures for the magnetically driven ferroelectricity are much higher (120 K to 250 K) [8] compared to those of the respective rare-earth manganites (27 K in $TbMnO_3$). [9] For example, the G-type antiferromagnetic ordering (AFM) ordering of Cr-moments, coinciding with the onset of electric polarization, is observed below the Néel temperature (T_N^{Cr}) of 157 K in $TbCrO_3$. [8] From neutron diffraction studies of $RCrO_3$ bulk samples it is known that Cr sublattice in each of these materials exhibit G-type AFM with a slight canting. [10] However, phenomenon of ferroelectricity and MF properties in these chromites are not yet well understood. For instance, ferroelectric-paraelectric transitions (as evidenced by pyroelectric current measurements) of a few $RCrO_3$ have recently been reported at their T_N^{Cr}, categorizing these as Type II ME MFs. [8] Whereas, a few earlier studies on $RCrO_3$ (for R = Tb, Dy, Ho, Er, Yb, Lu, and Y) reported such ferroelectric transitions (non-zero electric polarization) at higher temperatures than their T_N^{Cr}, which would place these materials in Type I ME MF category. [11,12] Further, in $ErCrO_3$, ferroelectric polarization was found to appear at $T_N^{Cr} \approx 133$ K and disappear at 22 K, the spin re-orientation temperature (T_{SR}), below which the weak ferromagnetism (FM) associated with the Cr-sublattice also disappears. [8] However, even though $SmCrO_3$ showed T_{SR} (as in $ErCrO_3$), no such disappearance of ferroelectric polarization was observed. [8] Evidently there are discrepancies in multiferroic properties of $RCrO_3$ compounds and the mechanism for the magnetic driven ferroelectricity is not clear. Thus, more studies are needed in order to clarify the ordering behaviors of this class of materials. From current literature, it is obvious that a crucial first step in interpreting the electric properties of these bulk $RCrO_3$ materials is to have a clear understanding of their magnetic behavior. The

complex interactions between the two kinds of magnetic ions (R^{3+} and Cr^{3+}) exhibit a variety of magnetic phenomena in these compounds. Even though it is clear that the magnetic moment of the R-ion also plays a role in determining the ferroelectric properties of $RCrO_3$ (no polar order when R is non-magnetic) [8]; it is not clear how the different magnetic transitions and interactions in such chromites will be modified with the substitution of a non-magnetic, a significantly magnetic, or a strongly magnetic R-ion, as has been studied in $TbMnO_3$. [13–16] Such studies could lead to not only improved insights into magnetic interactions but also shed light into the mechanism of magnetically driven ferroelectricity, which can further lead to an enhancement of their electric polarization values.

In this work, $DyCrO_3$ (DCO) was chosen as a parent compound due to the high magnetic moment of Dy^{3+} and prepared by citrate method. The Y^{3+}, Er^{3+}, and Ho^{3+} were substituted for Dy^{3+} in DCO serving as the non-magnetic, significantly magnetic, and strongly magnetic substituting ions, respectively. To the best of our knowledge, this is the first report on the magnetic properties of the A-site rare-earth substitution in $RCrO_3$.

II. Synthesis and Structural Characterization:

In order to prepare DCO and $Dy_{0.7}R_{0.3}CrO_3$ (for R=Y, Er, and Ho, hereafter referred to as DYCO, DECO, and DHCO), a citrate chemical solution route was used. Stoichiometric ratios of nitrates of Dy, Y, Er, Ho, and Cr were first dissolved in water at 70°C followed by the addition of citric acid. These solutions were then dried and annealed at 900°C for 2 hours in an O_2 environment. Powder X-ray diffraction (XRD) measurements were performed on a Bruker D5 diffractometer using Cu-Kα radiation. Raman spectroscopy measurements were taken using a 514 nm wavelength Argon laser. The XRD and Raman spectroscopy data were utilized to evaluate the structural properties and phase purity of the samples. DC magnetization values were measured using the Vibrating Sample Magnetometer (VSM) option attached to the Evercool Physical Property Measurement System (from Quantum Design).

Table I: Table I shows the magnetic moment (μ), ionic radii (r), and atomic mass (m) of the rare-earth and Cr ions relevant to this study. Note that the rare-earth ionic radii here are compared in 9-fold coordination, whereas the Cr ion is presented in 6-fold coordination.

	Dy^{3+}	Y^{3+}	Er^{3+}	Ho^{3+}	Cr^{3+}
μ^a (μ_B)	10.65	0	9.58	10.61	3.87
r^b (Å)	1.083	1.075	1.062	1.072	0.615
m^c (u)	162.5	88.9	167.3	164.9	52.00

[a] References [17,18].
[b] Reference [19].
[c] Reference [20].

DCO has been shown to form in an orthorhombically distorted perovskite (ABO_3) structure with space group *Pbnm*. [10] The Dy^{3+} at the A-site of the structure has 12-fold coordination, while the Cr^{3+} ions are located at the octahederally coordinated B-sites. The XRD

measurements are presented in Fig. 1 to demonstrate the effect of the chemical substitution on the structure of DCO. It is noted that in spite of similarities in the ionic radii of the substituted ions (presented in Table I), the shifts in the positions of the XRD peaks of these compounds (relative to the positions observed in pure DCO) could be detected reflecting the change in lattice parameters (as presented in Table II). The lattice parameters were calculated from peak fittings of the (020), (022), and (202) reflections in the XRD θ-2θ scans. Table II also presents the lattice parameters of $YCrO_3$, $ErCrO_3$ and $HoCrO_3$ reported earlier. [21] The lattice parameters of all the substituted samples are between the lattice parameters of DCO and those of the respective pure $RCrO_3$ compound. It is worth noting that no additional Bragg lines due to secondary phases were detected in the substituted powder samples, confirming the effectiveness of this solution based synthesis to prepare single phase samples. The full widths at half maximum of the XRD peaks, as determined by Pearson 7 peak fitting, were used to estimate the crystallite size using the Williamson-Hall analysis [22,23]:

$$\beta \cos(\theta) = \frac{K\lambda}{t} + \eta \sin(\theta) \quad (1)$$

where t is the crystallite size, K is the dimensionless shape parameter (0.89 was used in this study in accordance to earlier reports of synthesis of similar materials [24,25]), λ is the wavelength of the X-ray beam, and β is the full width at half maximum of the diffraction peak at the Bragg angle (θ), and η is the strain. The crystallite sizes determined by this method have large uncertainties arising from mean-squared-error between the data and the fitting to Equation 1. The crystallite sizes of all the present samples were found to be in the range of 90 - 200 nm (Fig. 2a) signifying essentially bulk-like materials. The large uncertainties in the magnitudes of t evident in Fig. 2a result from the inherent weakness of the XRD method to accurately determine crystallite sizes greater than about 50 nm as the widths of the lines become smaller for larger sizes. The present samples have larger crystallite sizes than that reported for hydrothermally synthesized $GdCrO_3$. [26] It should be noted that each of these samples were found to have less than 1% compressive strain (Fig. 2b). This lattice strain likely results from distribution of defects caused by the synthesis route. [27] Additionally, the substitutions in the present samples will affect the strain state.

Table II: The lattice parameters (a, b, and c), and unit cell volume (V) of the presents samples. The lattice parameters of the pure $RCrO_3$ compounds are also presented here.

	Samples (present study)				Pure $RCrO_3$[d]		
	DCO	DYCO	DECO	DHCO	$YCrO_3$	$ErCrO_3$	$HoCrO_3$
a (Å)	5.276	5.266	5.263	5.261	5.255	5.214	5.243
b (Å)	5.529	5.526	5.529	5.521	5.52	5.503	5.533
c (Å)	7.555	7.542	7.546	7.547	7.536	7.504	7.534
V ($Å^3$)	220.379	219.501	219.585	219.176	218.606	215.303	218.554

[d] Reference [21].

The Raman spectra of the four samples measured at room temperature are compared in Fig. 3. The orthorhombic *Pbnm* structure (or equivalently *Pnma* by a shift of indices) of $RCrO_3$ materials such as $DyCrO_3$ has 24 Raman active modes: $\Gamma_{Raman} = 7A_g + 5B_{1g} + 7B_{2g} + 5B_{3g}$. [28] In the chromites as well as the orthorhombic manganites, most of these phonon modes shift to low frequency with the increase in the ionic radii of the R-ion. [21,29] These Raman modes are sensitive not only to changes in the average ionic radii, but also to changes in the average atomic mass. [21] The sensitivity to atomic mass can be used to confirm substitutions in to the parent compound, as seen in the Raman spectra of the present samples (Fig. 3). This is especially evident in the case of the present DYCO sample. While the atomic radii of all the substitute ions used in this study are similar, Y^{3+} is a much lighter element than Dy^{3+}, Er^{3+}, or Ho^{3+}. Therefore, Y^{3+} substitution is expected to significantly shift the position of Raman peaks whose corresponding phonon modes strongly depend on the A-site atomic mass. It should be noted that if there was any phase separation (i.e. Dy^{3+}-rich and substitute-rich regions within the bulk), mode splitting could be expected. [30] However, in the present samples no such mode splitting is observed. In an earlier Raman scattering study of pure $RCrO_3$ compounds, it was found that the first A_g and B_{2g} modes in the Raman spectrum strongly depend on the A-site atomic mass. [21] For $DyCrO_3$ and $HoCrO_3$, the first A_g and B_{2g} modes in both compounds were found at ≈ 141 cm^{-1} and 161 cm^{-1}, while for $YCrO_3$ these two modes were reported at 185 cm^{-1} and 218 cm^{-1}, respectively. [21] Thus, in the present sample, Y^{3+} substitution is expected to shift the first A_g and B_{2g} modes to higher wavenumbers as compared to those in pure $DyCrO_3$. This is the case for the present DYCO sample, as observed and plotted in Fig. 1b. The Raman spectra for DECO and DHCO samples show only small deviations in the positions of the phonon modes from those observed in DCO. The results of the Raman spectroscopy measurements further corroborate the phase purity of each sample as seen in the XRD measurements.

III. Results from Magnetic Measurements and their Discussion:

A. Temperature dependence of magnetic susceptibilities:

The temperature dependence of the magnetization of the pure and rare-earth ion substituted DCO samples in a measuring field H = 50 Oe for the zero-field cooled (ZFC) and field cooled (FC) cases are shown in Fig. 4. There are substantial changes in the measured magnetization as a result of substitution of DCO. For example, Y^{3+} substitution decreases the magnitude of the FC magnetization at all temperatures (see Fig.4b) as compared to that of pure DCO (see Fig. 4a). Such behavior is expected due to the non-magnetic nature of the Y^{3+} ion. Er^{3+} on the other hand is magnetic, which leads to a similar, but slightly higher, magnetization compared to DCO, as observed in the FC data (Fig. 4c) Unlike Dy^{3+}, Er^{3+} moments are known to antialign with the net Cr^{3+} moments in $ErCrO_3$. [10] Thus, in the present DECO sample two competing R^{3+}-Cr^{3+} exchange interactions are expected. It is noted that there is a distinct change in slope in the FC data for DECO at ≈ 7.5 K indicating the onset of a magnetic transition. In $ErCrO_3$, a spin reorientation transition of the Cr^{3+} moments was reported at 22 K, which is

thought to be caused by the strong Er^{3+}-Cr^{3+} interaction. [8,10] Therefore, in the present case it can be concluded that the R^{3+}-Cr^{3+} interaction is strongly modified (relative to DCO) by the substitution of Er^{3+}.

The FC magnetization values of the DHCO sample (as shown in Fig. 4d) are higher than those of DCO sample. The higher magnetization of the Ho^{3+} substituted sample seems to suggest cooperative alignment between Ho^{3+} moments and the net Cr^{3+} moments. Reports of ZFC measurements in pure $HoCrO_3$ show negative magnetization, which was believed to be caused by a small antialigning Ho^{3+}-Cr^{3+} interaction. [31,32] Su *et al*. [31] posit that with no applied magnetic field, the Ho^{3+} ions antialign to the weak ferromagnetic signal from the Cr^{3+} sublattice; this antialignment is then overcome in the FC measurements by the strength of the measuring field (100 Oe used in Ref. [31]). In the present DHCO sample, since Dy^{3+} and Ho^{3+} have similar magnetic moments, a more complete alignment of the rare-earth moments to the Cr^{3+} contribution is needed to explain the higher magnetization in the FC measurements of DHCO as compared to DCO. In the ZFC measurements the magnetization of DHCO is somewhat smaller than in DCO. Therefore, in the case of the present DHCO sample it can be concluded (following the interpretation of Su *et al*. [31]) that the Ho^{3+}-Cr^{3+} interaction tends to antialign the Ho^{3+} and Cr^{3+} moments, but is overcome at low applied fields (50 Oe in present case) leading to co-alignment.

For an accurate determination of the T_N^{Cr} of the present samples, the susceptibility times the temperature (χT) values and its derivative with respect to temperature $\{d(\chi T)/dT\}$ were plotted against T as shown in Fig. 5. The temperature variation of this term, $d(\chi T)/dT$, is similar to the variation of the heat capacity in antiferromagnets and therefore it provides an accurate measure of the magnetic ordering temperature. [22,33,34] As the lattice parameters (and chemical compositions) of the present samples were modified through chemical substitution, it is expected that the Néel temperatures were affected as well. As mentioned earlier, the magnetic ordering of $RCrO_3$ materials are quite similar and the T_N^{Cr} values of the pure $RCrO_3$ compounds (for R = Dy, Y, Er, Ho) are only a few degrees apart. [10,32,35] In an earlier study, the T_N^{Cr} in $DyCrO_3$, $YCrO_3$, $ErCrO_3$, and $HoCrO_3$ were reported to be at 147 K, 140 K, 135 K, and 140 K, respectively. [35] In the present samples, there were only slight changes in the lattice parameters and correspondingly slight changes in the observed T_N^{Cr} values (presented in Table III). Each of the substituents used in this study have a smaller ionic radius than that of Dy^{3+} and caused a slight decrease in the T_N^{Cr}.

In most materials, the temperature dependence of the magnetic susceptibility data well above T_N can be fitted to the Curie-Weiss law. However, in the present material system, near the T_N^{Cr}, the susceptibility can deviate from this behavior. This deviation was modeled by Moriya for the case of weak ferromagnets (canted antiferromagnets) to account for the antisymmetric exchange interaction now known as the Dzyaloshinskii-Moriya (DM) interaction. [36] Parallel to

the easy magnetization axis of the crystal the susceptibility follows the Curie-Weiss law. However, perpendicular to the easy axis the susceptibility χ must account for the DM interaction. Since the present samples are powder (polycrystalline) samples, it is not possible to independently measure parallel and perpendicular susceptibilities; thus the effect of the perpendicular χ will be dominant for the powder sample. Therefore, we have modeled the measured powder susceptibility by Eq. 2 with the $(T - T_0)/(T - T_N)$ resulting from the effect of the DM interaction [34].

$$\chi = \frac{C}{(T-\Theta)} \frac{(T-T_0)}{(T-T_N^{Cr})} \tag{2}$$

where χ is the total DC susceptibility of the sample, T is the temperature, C is the Curie constant, Θ is the Weiss temperature, T_N^{Cr} is the Néel temperature for Cr ordering as mentioned before, and T_0 is a fitted parameter. For the data of each sample above T_N^{Cr}, the data of inverse χ vs. T was fitted to Eq. (2) with the fitting shown in Fig. 6 and the evaluated parameters listed in Table III. The excellent fits evident in Fig. 6 resulting from combining the parallel and perpendicular contributions to the susceptibility into a single term for the powder sample, as in Equation 2, ensures uniqueness of the fits. The parameters C, T_N^{Cr}, and T_0 were all taken as adjustable parameters of the fitting and the extracted values are also presented on Table III. It should be noted that the T_N^{Cr} value as obtained by the $d(\chi T)/dT$ method agree with those acquired from the modified Curie-Weiss law presented earlier. It is noted that the effect of the $(T - T_0)/(T - T_N^{Cr})$ term in Eq. (2) is important only near T_N^{Cr} resulting in the sharp drop in inverse χ because the difference between T_N^{Cr} and T_0 is less than one degree.

Information about the exchange interactions (J_e) between Cr^{3+} ions (Cr^{3+}-Cr^{3+} interactions) can be extracted from the parameters obtained in the aforementioned modified Curie-Weiss law. The other exchange interactions present in the samples (such as the R^{3+}-R^{3+} and R^{3+}-Cr^{3+} interactions) will not contribute to the information contained in T_N^{Cr} and T_0 since the Cr^{3+} ordering temperature is well above the Dy^{3+} ordering temperature. Following Moriya [34], expressions for T_N^{Cr} and T_0

$$T_0 = \frac{2J_e Z S(S+1)}{3k_B} \tag{3}$$

$$T_N^{Cr} = \frac{2J_e Z S(S+1)}{3k_B} \left[1 + \left(\frac{D}{2J_e}\right)^2\right]^{1/2} \tag{4}$$

can be used to provide semi-quantitative analysis of the strength of symmetric (J_e) and antisymmetric (D) exchange interactions only between Cr^{3+} ions. In equations 3 and 4, Z is the coordination of Cr^{3+} with respect to Cr^{3+} (*i e.* 6 in the present case), $S = 3/2$ is the spin quantum

number of Cr^{3+}, and k_B is Boltzmann's constant. Each of the substitutions in the Dy-site resulted in a slight reduction in the J_e reflecting the similar drop in T_N^{Cr} value. The estimated magnitudes of D in Table III are about 20 % of the magnitudes of J_e and are nearly the same for all the four samples

The Weiss constants as obtained from the fitting to the aforementioned modified Curie-Weiss law are negative for each of the present samples, indicating AFM order as expected. The effective magnetic moment (μ_{eff}) of the present sample is calculated from the Curie constant using:

$$C = \frac{N\mu_{eff}^2}{3k_B} \tag{4}$$

where N is Avogadro's number and k_B is the Boltzmann constant. Ho^{3+} and Dy^{3+} have similar magnetic moments, and therefore μ_{eff} of the DCO and DHCO samples were found to be similar. Er^{3+} has comparatively smaller magnetic moment that resulted in the reduction of the μ_{eff} of the DECO sample. The non-magnetic Y^{3+} ion substitution has the largest impact resulting in a significant reduction of the μ_{eff} of the DYCO sample. As presented in Table III, the observed magnetic moment values of the present samples are close to those estimated from the free-ion moments using the equation:

$$\mu_{eff} = \left[(1-x)\mu_{Dy}^2 + (x)\mu_R^2 + \mu_{Cr}^2\right]^{1/2} \tag{5}$$

where x = 0.3 for the substituted samples and the magnetic moments of different ions are from Table I.

Table III: The magnetic parameters resulting from fitting the susceptibility data to Equation 2. The Néel temperature T_N^{Cr} (K), the fitting parameter T_0 (K), the symmetric exchange constant J_e (K), the antisymmetric exchange constant D (K), the Weiss temperature Θ (K), Curie constant C (emu K Oe^{-1} mol^{-1}), and effective magnetic moments μ_{eff} (μ_B).

	DCO	DYCO	DECO	DHCO
T_N^{Cr} †	145.0	142.3	140.8	143.4
T_N^{Cr}	144.98 ± 0.04	142.93 ± 0.04	140.97 ± 0.03	143.90 ± 0.04
T_0	144.1 ± 0.1	142.2 ± 0.1	140.3 ± 0.1	143.1 ± 0.1
J_e	9.608 ± 0.007	9.479 ± 0.006	9.351 ± 0.005	9.542 ± 0.007
D	2.1 ± 0.1	1.9 ± 0.1	1.9 ± 0.1	2.0 ± 0.1
Θ	-61 ± 7	-48 ± 5	-52 ± 5	-59 ± 6
C	17.2 ± 0.4	10.3 ± 0.2	15.3 ± 0.3	16.3 ± 0.3
μ_{eff}	11.7 ± 0.1	9.08 ± 0.09	11.1 ± 0.1	11.4 ± 0.1
μ_{eff} ‡	11.312	9.699	11.03	11.304

† The Néel temperature T_N^{Cr} (K) as measured by the $d(\chi T)/dT$ method.

‡ The effective magnetic moment as estimated by Equation 5.

B. Hysteresis loop parameters and their temperature dependence:

Isothermal magnetization (M) versus applied magnetic field (H) loops were acquired at select temperatures between 5 K and 160 K (in steps of 5 K) and in magnetic fields up to 40 kOe. Representative hysteresis loops for the four samples at one temperature viz. 60 K are shown in Fig. 7. The magnetic hysteresis loops for all the four samples investigated here viz. DCO, DYCO, DECO, and DHCO show the presence of a weak ferromagnetic component (M_{WF}) and a linear component, with M_{WF} not saturating till about 25 kOe. Following the analysis of the data above T_N, the origin of M_{WF} is related to the canting of the Cr^{3+} spins, whereas the linear component is clearly evident above 25 kOe in the plots of Fig. 7. The linear component contains contributions from the antiferromagnetic susceptibility of the Cr^{3+} sub-lattice and paramagnetic (and antiferromagnetic) susceptibility of the R^{3+} ions above (and below) their ordering temperatures. In addition to Cr^{3+}-Cr^{3+} exchange interactions determined in Table III from the analysis of the paramagnetic susceptibility, the other weaker exchange interactions of R^{3+}-R^{3+} ions and R^{3+}-Cr^{3+} need to be considered in discussing the properties at lower temperatures.

The temperature dependence and sample to sample variance of the magnetic remanence (M_R) obtained from the hysteresis loops (of the form given in Fig. 7) are shown in Fig. 8a-b, respectively. It should be noted that the temperature dependence of the M_R in each sample follows a similar trend to the FC measurements discussed earlier, with DHCO showing the strongest magnetization and DYCO showing the weakest. Additionally, the temperature dependence and sample to sample variance of the coercivity (H_C) were also obtained from the isothermal magnetization measurements and are shown in Fig. 9a-c, respectively. For H_C, the temperature dependence has a general trend with decrease in temperature below T_N^{Cr}: H_C first increases reaches a broad plateau, and then decreases with further decrease in temperature. Such a broad peak in the temperature dependence of H_C data was recently reported for pure DCO bulk [37] and was qualitatively interpreted on the basis of superimposing Cr^{3+} and Dy^{3+} magnetic sub-lattices. [37,38] There are two aspects of these results, which require interpretation viz. variations with temperature and variations with substitution across the samples. In all cases, the present rare-earth substitutions in DCO lead to an increase in H_C values (in the plateau region) as compared to that of pure DCO.

Looking at the temperature variation data, the initial increase in H_C with decrease in temperature below T_N^{Cr} in Fig. 9a is due to the well–known temperature dependence of magneto-crystalline anisotropy constant (K_A). [39] In the Stoner-Wohlfarth (SW) model for a single-domain magnetic particle, H_C is directly proportional to the magneto-crystalline anisotropy. [39] In systems with uncompensated moments but without magnetic impurities, continuous increase in H_C with decrease in temperature below T_N or T_C has been reported. [40,41] In the SW model, H_C is related to K_A by the equation: $H_C = (K_A / M_S)$, where M_S is the saturation magnetization. The $M_S = 0$ at and above T_N and for $T < T_N$, M_S has the approximate temperature dependence of the Brillouin function. In addition, it is known that the temperature dependence of $K_A \sim (M_S)^n$

where n can be as large as 10 [39] and it is often system dependent. Thus, from magneto-crystalline anisotropy alone, H_C value should continue to increase with decrease in temperature below T_N^{Cr}.

Experimentally, the temperature dependence of H_C in the present material systems (Fig. 9a) shows a plateau followed by the reduction of H_C values at lower temperatures. Therefore, an additional mechanism has to be operative here to yield such variation. It is known that in a system with domain walls, coercivity can also be strongly affected by defects, grain boundaries, and other imperfections, which might pin-down the domain walls and hence impede domain rotation as the magnetic field is varied. [18] In the present case, all our samples were synthesized using the same process resulting in essentially similar crystallite (grain) sizes of about 100 nm or larger and similar strains (see Fig. 2). Although, the presence of strain and smaller grain sizes are known to increase H_C [42], these are likely not the reason for increase in H_C with substitution in the present samples. Instead, the sample to sample increase in H_C (as shown in Fig. 9b-c) is likely to be due to the dopant ions with their different magnetic moments acting as impurities and impeding the rotation of exchange-coupled Cr^{3+} moments. The R^{3+} ions can also exhibit a single-ion anisotropy related to the strength of the quadrupole moments of the partially filled *f*-obitals. The trend in quadrupole moments for the R^{3+} ions reported by Skomski [43] does not correlate with the H_C trends seen in Fig. 9. However, at lower temperatures the weaker R^{3+}-Cr^{3+} exchange coupling becomes operative due to lowering of the thermal energy. Thus, the magnetic moment of the dopants can now rotate with the Cr^{3+} moment thus lowering the measured H_C. This effect becomes increasingly important with decrease in temperature, providing a qualitative interpretation of the data in Fig. 9. In the sample to sample variation of H_C at different temperatures in Fig. 9b, the observed decrease of H_C at 5 K and 10 K for DECO sample support this argument since below about 10 K, Er^{3+} moments become ordered antiferromagnetically. Substituting non-magnetic Y^{3+} for Dy^{3+} in $DyCrO_3$ resulted in larger peak coercivity (as seen in Fig. 9) since the ferromagnetic Cr^{3+} sublattice contributes a larger portion of the net magnetization. The stronger exchange interaction of Ho^{3+} with Cr^{3+} is likely responsible for the largest change in H_C across the samples in Fig. 9b-c. The isotropic exchange interactions cannot contribute to the coercive field, [18] it can be concluded that the Er^{3+} and Ho^{3+} substitutions increase the anisotropic component (*i.e* the DM interaction) of the exchange interactions. From our analysis of the M vs. T data summarized in Table III, the $D_{Cr\text{-}Cr}$ remains constant across the samples. The R^{3+}-R^{3+} is weak and not expected to significantly affect the magnetic properties above the rare-earth ordering temperature, [44,45] leaving only anisotropic component of the R^{3+}-Cr^{3+} interaction to account for the observed differences in the coercive fields of the present samples. This is consistent with previous optical absorption studies, which found that the DM interaction dominates the Er^{3+}-Cr^{3+} and Ho^{3+}-Cr^{3+} interactions in the respective compounds. [46,47] These studies show important information on the fundamental magnetic exchange parameters of DCO and $Dy_{0.7}R_{0.3}CrO_3$ (for R=Y, Er, and Ho) obtained from simple magnetization measurements.

IV. Conclusions:

In summary, a solution based citrate route provided a facile synthesis route for phase pure $DyCrO_3$ and $Dy_{0.7}R_{0.3}CrO_3$ (for R=Y, Er, and Ho) as confirmed by X-ray diffraction and Raman spectroscopy techniques. The temperature dependent DC magnetic measurements revealed only slight changes to the Néel temperatures with rare-earth substitutions in $DyCrO_3$. These slight changes are reflected in the isotropic exchange interaction (J_e) (between Cr^{3+} ions) values obtained from fitting to Dzyaloshinskii-Moriya interaction modified Curie-Weiss law. An estimation of the strength of the Dzyaloshinskii-Moriya interaction (D) was also obtained. This small D (between Cr^{3+} ions) was found to be unaffected by the rare-earth substitutions. Successive isothermal magnetization measurements revealed a plateau in the temperature dependence of the coercivity in each of the samples. The decrease in coercivity at the lower temperatures is interpreted in terms of exchange coupling of the R^{3+} sublattice to the Cr^{3+} sublattice. The increase in coercivity in the measured temperature range in the Er^{3+} and Ho^{3+} substituted samples compared to the pure $DyCrO_3$ sample is attributed to the variance of the Dzyaloshinskii-Moriya component of the R^{3+}-Cr^{3+} interactions.

Acknowledgments

This work is based in part upon the work supported by the National Science Foundation grant DMR # 1310149 and Large Grant from the University of Connecticut.

References:

[1] D. Khomskii, Physics (College. Park. Md). **2**, 20 (2009).

[2] D. I. Khomskii, J. Magn. Magn. Mater. **306**, 1 (2006).

[3] S.-W. Cheong and M. Mostovoy, Nat. Mater. **6**, 13 (2007).

[4] M. Staruch, G. Lawes, A. Kumarasiri, L. F. Cotica, and M. Jain, Appl. Phys. Lett. **102**, 062908 (2013).

[5] M. Staruch, D. Violette, and M. Jain, Mater. Chem. Phys. **139**, 897 (2013).

[6] C. Binek and B. Doudin, J. Phys. Condens. Matter **17**, L39 (2005).

[7] X. Chen, A. Hochstrat, P. Borisov, and W. Kleemann, Appl. Phys. Lett. **89**, 202508 (2006).

[8] B. Rajeswaran, D. I. Khomskii, A. K. Zvezdin, C. N. R. Rao, and A. Sundaresan, Phys. Rev. B **86**, 214409 (2012).

[9] T. Kimura, T. Goto, H. Shintani, K. Ishizaka, T. Arima, and Y. Tokura, Nature **426**, 55 (2003).

[10] R. Hornreich, J. Magn. Magn. Mater. **7**, 280 (1978).

[11] H. B. Lal, R. D. Dwivedi, and K. Gaur, J. Mater. Sci. Mater. Electron. **7**, 35 (1996).

[12] J. R. Sahu, C. R. Serrao, N. Ray, U. V. Waghmare, and C. N. R. Rao, J. Mater. Chem. **17**, 42 (2007).

[13] A. Kumar, P. Shahi, S. Kumar, K. K. Shukla, R. K. Singh, A. K. Ghosh, A. K. Nigam, and S. Chatterjee, J. Phys. D. Appl. Phys. **46**, 125001 (2013).

[14] T. Arima, T. Goto, Y. Yamasaki, S. Miyasaka, K. Ishii, M. Tsubota, T. Inami, Y. Murakami, and Y. Tokura, Phys. Rev. B **72**, 100102 (2005).

[15] T. Goto, Y. Yamasaki, H. Watanabe, T. Kimura, and Y. Tokura, Phys. Rev. B **72**, 220403 (2005).

[16] C. L. Lu, S. Dong, K. F. Wang, and J.-M. Liu, Appl. Phys. A **99**, 323 (2009).

[17] J. Jensen and A. Mackintosh, *Rare Earth Magnetism: Structures and Excitations Clarendon* (Clarendon Press, Oxford, 1991).

[18] J. Coey, *Magnetism and Magnetic Materials* (Cambridge University Press, New York, 2010).

[19] R. D. Shannon, Acta Crystallogr. Sect. A **32**, 751 (1976).

[20] M. E. Wieser, Pure Appl. Chem. **78**, 2051 (2006).

[21] M. C. Weber, J. Kreisel, P. A. Thomas, M. Newton, K. Sardar, and R. I. Walton, Phys. Rev. B **85**, 054303 (2012).

[22] P. Dutta, M. S. Seehra, S. Thota, and J. Kumar, J. Phys. Condens. Matter **20**, 015218 (2008).

[23] G. . Williamson and W. . Hall, Acta Metall. **1**, 22 (1953).

[24] S. Farhadi, Z. Momeni, and M. Taherimehr, J. Alloys Compd. **471**, L5 (2009).

[25] J. Ding, X. Lü, H. Shu, J. Xie, and H. Zhang, Mater. Sci. Eng. B **171**, 31 (2010).

[26] A. Jaiswal, R. Das, S. Adyanthaya, and P. Poddar, J. Nanoparticle Res. **13**, 1019 (2010).

[27] A. Khorsand Zak, W. H. Abd. Majid, M. E. Abrishami, and R. Yousefi, Solid State Sci. **13**, 251 (2011).

[28] M. N. Iliev, M. V. Abrashev, H.-G. Lee, V. N. Popov, Y. Y. Sun, C. Thomsen, R. L. Meng, and C. W. Chu, Phys. Rev. B **57**, 2872 (1998).

[29] M. N. Iliev, M. V. Abrashev, J. Laverdière, S. Jandl, M. M. Gospodinov, Y.-Q. Wang, and Y.-Y. Sun, Phys. Rev. B **73**, 064302 (2006).

[30] Y. Sharma, S. Sahoo, W. Perez, S. Mukherjee, R. Gupta, A. Garg, R. Chatterjee, and R. S. Katiyar, J. Appl. Phys. **115**, 183907 (2014).

[31] Y. L. Su, J. C. Zhang, L. Li, Z. J. Feng, B. Z. Li, Y. Zhou, and S. X. Cao, Ferroelectrics **410**, 102 (2010).

[32] J. Prado-Gonjal, R. Schmidt, J.-J. Romero, D. Avila, U. Amador, and E. Morán, Inorg. Chem. **52**, 313 (2013).

[33] E. Bragg and M. Seehra, Phys. Rev. B **7**, 4197 (1973).

[34] M. E. Fisher, Philos. Mag. **7**, 1731 (1962).

[35] B. Tiwari, Structural, Optical and Magnetic Properties of LnCrO3 (Ln = La, Gd, Dy, Ho, Y and Er), Indian Institute of Technology Madras, 2012.

[36] T. Moriya, Phys. Rev. **120**, 91 (1960).

[37] A. McDannald, L. Kuna, and M. Jain, J. Appl. Phys. **114**, 113904 (2013).

[38] R. Aleonard, J. Appl. Phys. **39**, 379 (1968).

[39] A. H. Morrish, *The Physical Principles of Magnetism* (IEEE Press, 2001), pp. 310–320, 344.

[40] M. S. Seehra and V. Singh, J. Phys. Condens. Matter **25**, 356001 (2013).

[41] M. S. Seehra, V. Singh, S. Thota, B. Prasad, and J. Kumar, Appl. Phys. Lett. **97**, 112507 (2010).

[42] S. Singh, S. Munjal, and N. Khare, J. Magn. Magn. Mater. **386**, 69 (2015).

[43] R. Skomski, *Simple Models of Magnetism* (Oxford University Press, 2008), pp. 1–32.

[44] T. Yamaguchi, J. Phys. Chem. Solids **35**, 479 (1974).

[45] A. Jaiswal, R. Das, K. Vivekanand, T. Maity, P. M. Abraham, S. Adyanthaya, and P. Poddar, J. Appl. Phys. **107**, 013912 (2010).

[46] R. Courths and S. Hüfner, Zeitschrift Für Phys. B Condens. Matter **22**, 245 (1975).

[47] R. Courths and S. Hüfner, Zeitschrift Für Phys. B Condens. Matter **24**, 193 (1975).

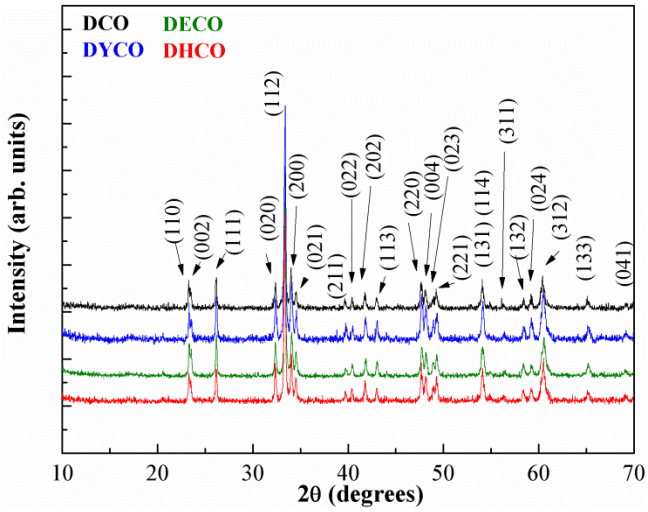

Figure 1: X-ray diffraction data of the present DCO and rare-earth substituted DCO samples.

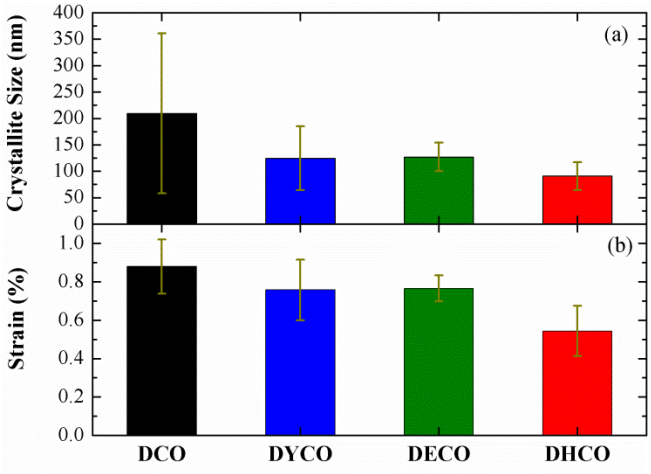

Figure 2: Histograms of the crystallite size (a) and strain (b) in the present powder samples, as determined by the Williamson-Hall analysis.

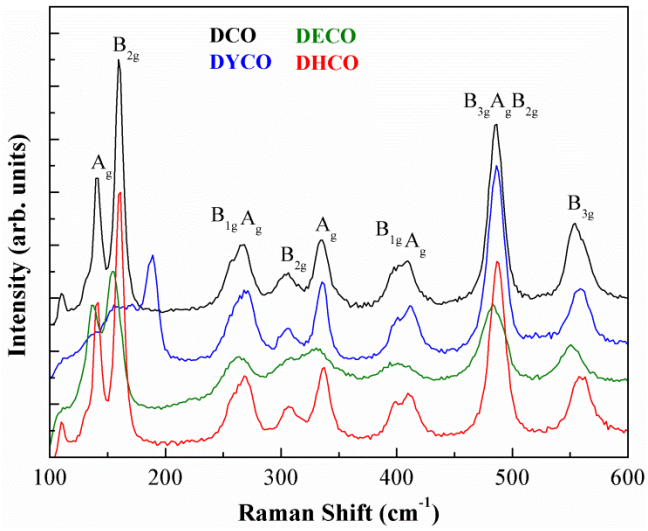

Figure 3: Raman spectra of the present DCO and Y, Er, and Ho doped DCO samples.

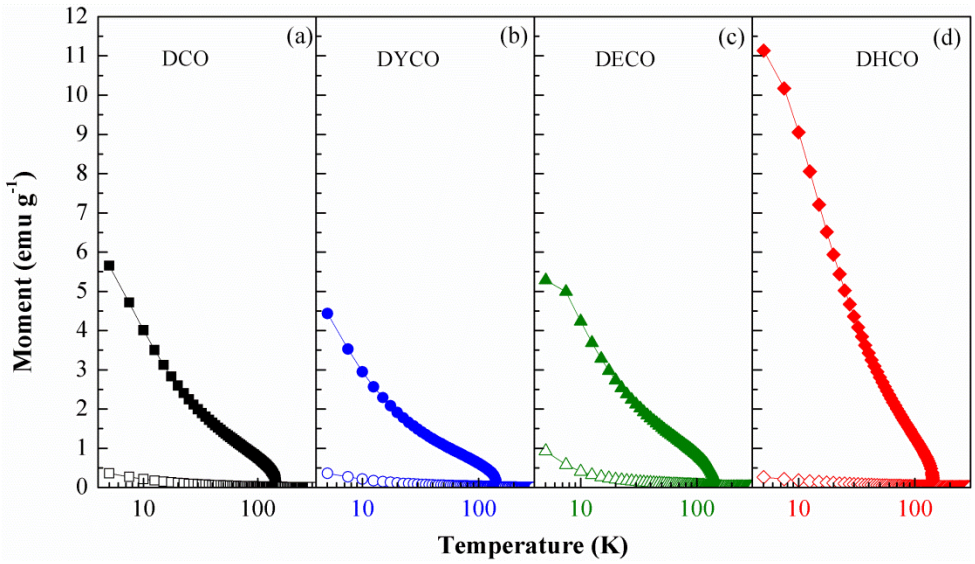

Figure 4: The temperature dependent zero field cooled (open symbols) and field cooled (closed symbols) dc magnetic measurements of DCO (a), DYCO (b), DECO (c), and DHCO (d) show how the magnetic behavior is affected by chemical substitution.

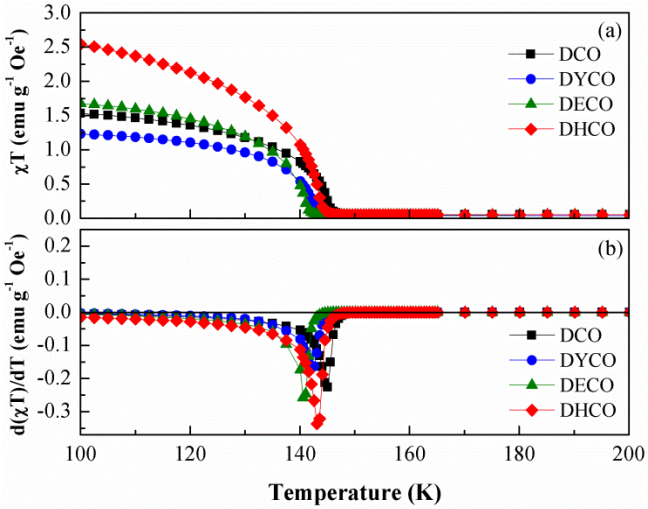

Figure 5: The temperature dependence of the magnetic susceptibility multiplied by the temperatuere (χT) (a) and its derivative $\{d(\chi T)/dT\}$ (b) using the field cooled magnetization values for each of the present samples. The peaks in (b) indicate the magnetic transition temperatures (Cr^{3+} ordering in this case).

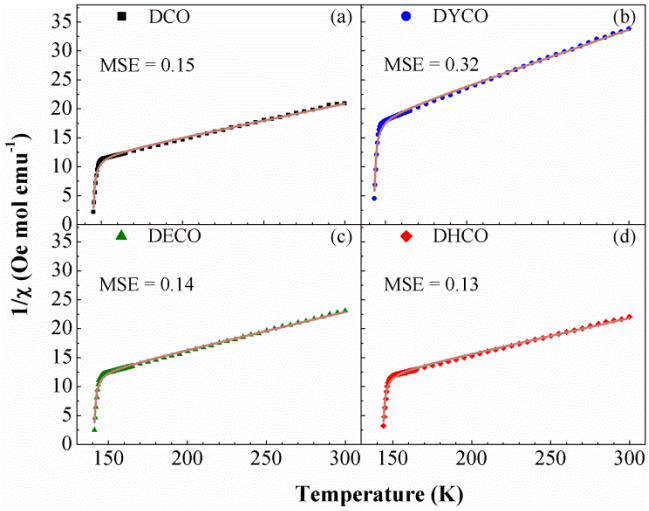

Figure 6: The temperature dependence of the inverse susceptibility ($1/\chi$) for the present pure and Y, Er, and Ho doped $DyCrO_3$ samples (a-d). Each plot shows the fitting to the Curie-Weiss law modified by the Dzyaloshinskii-Moriya interaction (solid line) from Equation 2 and the associated mean-squared-error (MSE).

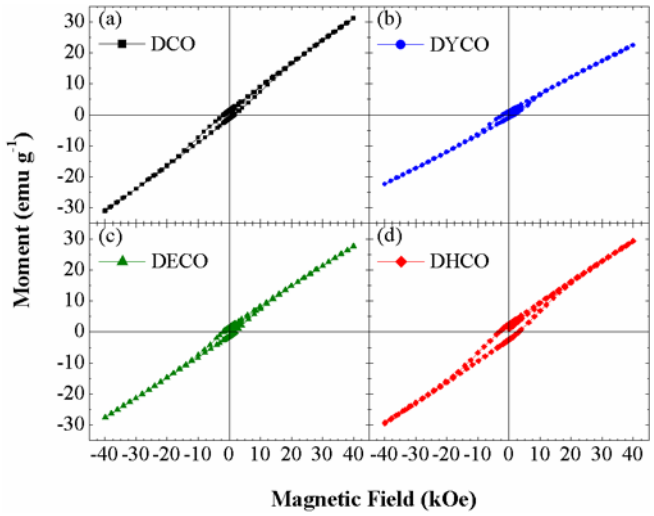

Figure 7: Isothermal magnetization measurements at 60 K for each of the present pure and Y, Er, and Ho doped $DyCrO_3$ samples (a-d). The magnetic behavior presented here is representative of the magnetic behavior observed at other temperatures.

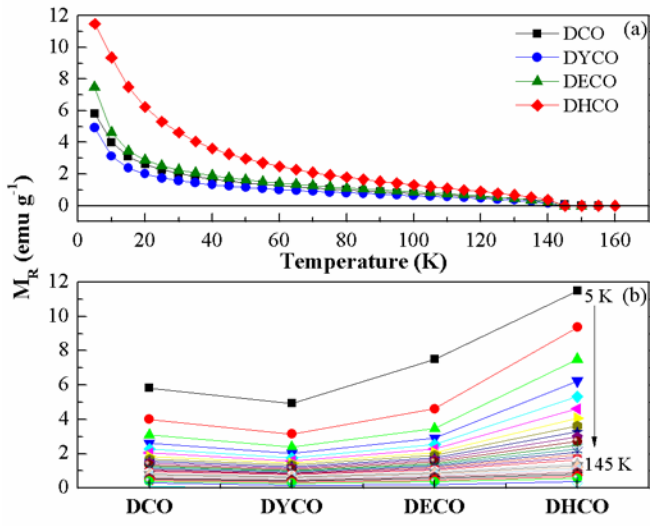

Figure 8: The temperature dependence (a) and sample to sample variance (b) of the remnant magnetization (M_R), as extracted from successive isothermal magnetization measurements.

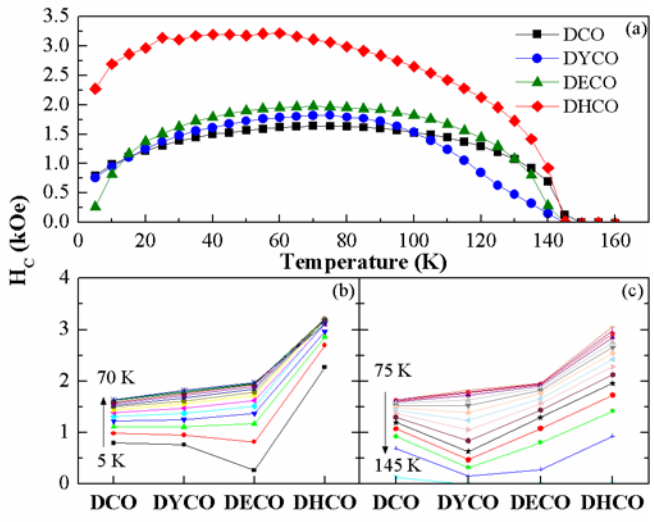

Figure 9: The temperature dependence (a) and sample to sample variance of the coercivity (H_C) at each temperature from 5 K to 70 K (b), and from 75 K to 145 K (b) in 5 K increments.